Electronic Supplementary Information for:

Shedding light on an ultra-bright photoluminescent lamellar gold thiolate coordination polymer, $[Au(p\text{-}SPhCO_2Me)]_n$

Christophe Lavenn,[a]§ Nathalie Guillou,[b] Miguel Monge,[c] Darjan Podbevšek,[d] Gilles Ledoux,[d] Alexandra Fateeva[e] and Aude Demessence*[a]

[a] Institut de Recherches sur la Catalyse et l'Environnement de Lyon (IRCELYON), Université Claude Bernard Lyon 1, CNRS, UMR 5256, Villeurbanne, France.

[b] Institut Lavoisier de Versailles (ILV), Université de Versailles Saint-Quentin-en Yvelines, CNRS, UMR 8180, Versailles, France.

[c] Departamento de Química, Universidad de La Rioja, Centro de Investigación en Síntesis Química (CISQ), Complejo Científico-Tecnológico, Logroño, Spain.

[d] Institut Lumière Matière (ILM), Université Claude Bernard Lyon 1, CNRS, UMR 5306, Villeurbanne, France.

[e] Laboratoire des Multimatériaux et Interfaces (LMI), Université Claude Bernard Lyon 1, CNRS, UMR 5615, Villeurbanne, France.

§ Current addresses: Institute for Integrated Cell-Material Sciences (iCeMS), Kyoto University, Japan; K. K. Air Liquide Laboratories, Tsukuba, Japan.

*aude.demessence@ircelyon.univ-lyon1.fr

Chem. Commun.

Experiments and methods

The crystal structure of (p-SPhCO$_2$Me)$_2$, compound **2**, was measured using Mo radiation (λ = 0.71073 Å) on an Oxford Diffraction Gemini diffractometer equipped with an Atlas CCD detector. Intensities were collected at 150 K by means of the CrysalisPro software.[1] Reflection indexing, unit-cell parameters refinement, Lorentz-polarization correction, peak integration and background determination were carried out with the CrysalisPro software. An analytical absorption correction was applied using the modeled faces of the crystal.[2] The resulting sets of hkl were used for structure solutions and refinements. The structure was solved by direct method with SIR97[3] and the least-squares refinement on F2 was achieved with the CRYSTALS software.[4] All non-hydrogen atoms were refined anisotropically. The hydrogen atoms were all located in a difference map, but those attached to carbon atoms were repositioned geometrically. The H atoms were initially refined with soft restraints on the bond lengths and angles to regularize their geometry (C···H in the range 0.93 –0.98 Å) and Uiso (H) (in the range 1.2–1.5 times Ueq of the parent atom) after which the positions were refined with riding constraints. Some selected crystallographic and refinement data are given in Table S1. CCDC-1441707 contains the supplementary crystallographic data. These data can be obtained free of charge from The Cambridge Crystallographic Data Centre via www.ccdc.cam.ac.uk/data_request/cif.

The structural determination of [Au(p-SPhCO$_2$Me)]$_n$, compound **1**, was carried out from powder X-ray diffraction data. Sample was introduced into a 0.5 mm capillary and spun during data collection to ensure good powder averaging. Pattern was scanned at room temperature on a Bruker D8 Advance diffractometer with a Debye-Scherrer geometry, in the 2θ range 3-100°. The D8 system is equipped with a Ge(111) monochromator producing Cu Kα1 radiation (λ = 1.540598 Å) and a LynxEye detector. All calculations of structural investigation were performed with the TOPAS program.[5] The LSI-indexing method converged unambiguously to an orthorhombic unit cell with satisfactory figure of Merit (M_{20} = 115). Unindexed lines observed on the powder pattern correspond to compound **2** as impurity. Given to the small amount of compound **2** in compound **1** (4.5 wt%), its presence did not prevent us to solve the structure of compound **1**. Structural investigation of [Au(SPhCO$_2$Me)]$_n$ was initialized by using the charge flipping method, which allowed location of gold atoms. The direct space strategy was then used to complete the structural model and the organic moiety has been added to the fixed gold atomic coordinates and treated as rigid body in the simulated annealing process. The position of the carbon atom of the methyl group was localized by difference Fourier map calculations. The final Rietveld plot (Fig. S5) corresponds to satisfactory model indicator and profile factors (Table S1). CCDC-1441706 contains the supplementary crystallographic data. These data can be obtained free of charge from The Cambridge Crystallographic Data Centre via www.ccdc.cam.ac.uk/data_request/cif.

Routine powder X-ray diffraction (PXRD) experiment was carried out on a Bruker D8 Advance A25 diffractometer using Cu Kα radiation equipped with a 1-dimensional position-sensitive detector (Bruker LynxEye). XR scattering was recorded between 4° and 90° (2θ) with 0.02° steps and 0.5 s per step (28 min for the scan). Divergence slit was fixed to 0.2° and the detector aperture to 189 channels (2.9°).

The infrared spectra were obtained from a Bruker Vector 22 FT-IR spectrometer with KBr pellets at room temperature and registered from 4000 to 400 cm^{-1}.

Thermo-gravimetric analyses (TGA) were performed with a TGA/DSC 1 STARe System from Mettler Toledo. Around 2 mg of sample was heated at a rate of 10 °C.min^{-1}, in a 70 μL alumina crucible, under air atmosphere (20 mL.min^{-1}). Shining droplets of bulk gold were observed at the end of experiment for compound **1**.

Sulphur percentage was determined by full combustion at 1320-1360 °C under O_2 stream and analysis of SO_2 and was titrated in a coulometric-acidimetric cell. Carbon and hydrogen percentages were determined by full combustion at 1030-1070 °C under O_2 stream and transformed into CO_2 and H_2O and were titrated on a coulometric detector. Analysis precision is 0.3 % absolute for carbon, sulphur and hydrogen.

SEM image was obtained with a FEI Quanta 250 FEG scanning electron microscope in the microscopy centre of Lyon 1 University. Sample was mounted on a stainless pad and sputtered with ~2 nm of a Au/Pd mixture to prevent charging during observation.

Solid-state NMR spectra were recorded on a Bruker DSX400 spectrometer. ^{13}C CPMAS (Cross Polarization - Magic Angle Spinning) experiments were carried out at 100.62 MHz in a 4 mm rotor spun at 10 kHz and ^{1}H MAS measurements were done at 400.16 MHz in a 2.5 mm rotor spun at 30 KHz. Data were collected using a standard one-pulse sequence with 3.05 µs (π/2) pulses for ^{13}C and with 2.8 µs (π/2) for ^{1}H. Chemical shifts were referred to tetramethylsilane (TMS).

X-ray photoelectron spectroscopy (XPS) experiment was carried out on a KRATOS Axis Ultra DLD spectrometer using monochromated Al Kα source (hν = 1486.6 eV, 150 W), a pass energy of 20 eV, a hybrid lens mode and an indium sample holder in ultra-high vacuum ($P < 10^{-9}$ mbar). The analyzed surface area was 300 µm × 700 µm. Charge neutralization was required for the sample. Scan survey was done at an energy of 160 eV and for the elements Au 4f, S 2p, O 1s and C 1s at 20 eV. The peaks were referenced to the aromatic carbon atoms components of the C 1s band at 284.7 eV. Shirley background subtraction and peak decomposition using Gaussian–Lorentzian products were performed with the Vision 2.2.6 Kratos processing program.

The photoluminescence studies were performed on a homemade apparatus. The sample was illuminated by a EQ99X laser driven light source filtered by a Jobin Yvon Gemini 180 monochromator. The exit slit from the monochromator was then reimaged on the sample by two 100m focal length, 2 inch diameter MgF_2 lenses. The whole apparatus has been calibrated by means of a Newport 918D Low power calibrated photodiode sensor over the range 190-1000 nm. The resolution of the system being 4 nm. The emitted light from the sample is collected by an optical fiber connected to a Jobin-Yvon TRIAX320 monochromator equipped with a cooled CCD detector. At the entrance of the monochromator different long pass filter can be chosen in order to eliminate the excitation light. The resolution of the detection system is 2 nm. Low temperature experiments were carried out in a closed chamber with liquid nitrogen flow. Condensation on the window was prevent with a nitrogen gas flow. Room temperature measurements were done after experiments at low and high temperature to check the reversibility the photoemission of the sample. No modification of the position and intensity was observed.

To perform luminescence lifetime measurements, the sample was excited by a pulsed laser diode from Hamamatsu, with a central wavelength at 379 nm, a peak power of 742 mW and pulses of 51 ps at room temperature. The repetition rate used for the experiment here was 50 kHz. The luminescence from the sample was collected with a lens, filtered by a high pass filter (FELH600 from Thorlabs) and fed to a PMA182 photomultiplier connected to a PicoHarp-300 TCSPC module both from picoquant. The overall timing resolution is in the order of 200 ps. Luminescence quantum yield (QY) was estimated at room temperature by comparing the sample $[Au(SPhCO_2Me)]_n$ to a porous silicon standard under the same geometrical conditions of complete excitation/emission mappings as described previously.[6] Three experiments have been carried out and give a mean QY of 70 ± 20 %.

Computational Details. DFT calculations were carried out using the Gaussian 09 package.[7] The following basis set combinations were employed for the metal Au: the 19-VE pseudo-potentials from Stuttgart and the corresponding basis sets augmented with two f polarization functions were used.[8] The C, O and S atoms were treated by Stuttgart pseudopotentials[9] including only the valence electrons for each atom. For these atoms double-zeta basis sets of ref 9 were used, augmented by d-type polarization functions.[10] For the H atoms, a double-zeta, plus a p-type polarization function was used.[11] DFT calculations were carried out using PBE1PBE functional.[12] All the DFT calculations were performed on model systems for complex 1 built up from their corresponding X-ray structures. Overlap populations between molecular fragments were calculated using the Gaussum program.[13] RI-MP2, RI-HF and RI-DFT/TDDFT calculations were carried out using TURBOMOLE version 6.4.[14] In the case of the RI-DFT/TDDFT calculations the hybrid PBE functional[15] was used together with the D3 dispersion correction previously described by Grimme.[16] In order to keep the computational cost feasible we have taken advantage of the Resolution of the Identity (RI) approximation for all the calculations performed with TURBOMOLE, which improves the computational efficiency of large-scale calculations.[17] All non-metal atoms were described by using a triple-zeta-valence quality basis sets with polarization function def-TZVP.[18] For gold we used the triple-zeta-valence quality basis sets with polarization function def2-TZVP.[19] In the case of gold the core electrons were described using a 60-electron relativistic effective core potential.[8] In the case of the full optimizations at RI-MP2 and RI-HF levels of theory we used the dinuclear model system $[\{Au(SPhCO_2Me)_2\}_2]^{2-}$. In order to prove the dispersive origin of the $Au(I)\cdots Au(I)$ interactions, the optimization has also been carried out at RI-Hartree-Fock (RI-HF) level of theory, where correlation is not included. In this case, repulsion between the $[Au(SPhCO_2Me)_2]^-$ is achieved and any local minimum is found, confirming the dispersive origin of the aurophilicity in this system. RI-DFT/TDDFT calculations were performed on the hexanuclear model $[Au_6(SPhCO_2Me)_8]^{2-}$ built up from the X-ray diffraction results. The lowest singlet-triplet ($S_0 \rightarrow T_1$) and the first 10 singlet-singlet electronic excitations ($S_0 \rightarrow S_n$) have been computed at RI-DFT/TDDFT level of theory for the representative model system $[Au_6(SPhCO_2Me)_8]^{2-}$, in which the aurophilic interactions are included (Fig. S23 and Tables S9-S10). The predicted excitation energies appear at 458 nm for the $S_0 \rightarrow T_1$ transition and from 425 to 391 nm for the singlet-singlet ones. Taking into account that the experimental phosphorescent excitation maximum appears at 370 nm, the slight red-shift of the computed values would be attributed to the anionic and non-polymeric nature of the model system $[Au_6(SPhCO_2Me)_8]^{2-}$. Nevertheless, a qualitative picture of the excitation process can be deduced from the character of the MOs involved in the computed excitations.

Chemicals. Tetrachloroauric acid trihydrate ($HAuCl_4.3H_2O$, ≥ 49 % Au basis) and methanol (Chromasolv®) were purchased from Sigma-Aldrich Company. 4-mercaptobenzoic acid (> 95 %) was ordered from TCI. The glassware used in the synthesis was cleaned with aqua regia (aqua regia is a very corrosive product and should be handled with extreme care), then rinsed with copious amount of distilled water and dried overnight prior to use. All reactions were carried out in atmospheric conditions.

Synthesis of 1 and 2: 4-mercaptobenzoic acid (735 mg, 4.77 mmol, 9 eq) was dissolved in methanol (65 ml) and heated at 80 °C. $HAuCl_4·3H_2O$ (190 mg, 0.53 mmol, 1 eq) was dissolved in 5 ml of methanol and added to the 4-mercaptobenzoic acid solution. The mixture was left to stir under reflux for 48 h during which time a white precipitate formed. The white solid **1** was isolated by filtration and washed with methanol and acetone and then dried in air. Yield: 174 mg (92 %). The filtrate of the first washing was left under atmospheric conditions and compound **2** crystalized as transparent needles after few days. Chemical Formula of **1**: $C_8H_7AuO_2S$; Molecular Weight: 364.17; Elemental Analysis (calc.) from ICPMS in wt%: C, 25.85 (26.38); H, 1.81 (1.94); S, 8.75 (8.80); gold content from TGA (calc.) wt%: 54.1, (54.09). Chemical Formula of **2**: $C_{16}H_{14}O_4S_2$; Molecular Weight: 334.41. Elemental Analysis (calc.) from ICPMS in wt%: C, 56.86 (57.47); H, 4.14 (4.22); S, 19.70 (19.18).

Table S1. Crystallographic data and Rietveld refinement parameters for **1** and **2** compounds.

Compound	**1**	**2**
State	Powder	Single crystal
Empirical formula	C8 H7 O2 S Au	C16 H14 O4 S2
M_r	364.18	334.42
Crystal system	Orthorhombic	Triclinic
Space group	*Pbca*	*P*-1
a (Å)	37.403(1)	5.9165(4)
b (Å)	7.0157(1)	7.6653(5)
c (Å)	6.3659(1)	17.8190(10)
α (°)	90	79.997(5)
β (°)	90	85.946(5)
γ (°)	90	75.915(6)
V (Å^3)	1670.45(7)	771.57(9)
Z	8	2
λ (Å)	1.540598	0.71073
Number of reflections	877	2691
No. of fitted structural parameters	21	199
Number of soft restraints	3	0
R_p, R_{wp}, R_{Bragg}	0.056, 0.076, 0.038	
R_1, wR_2		0.0351, 0.0605
GoF	6.41	0.9835

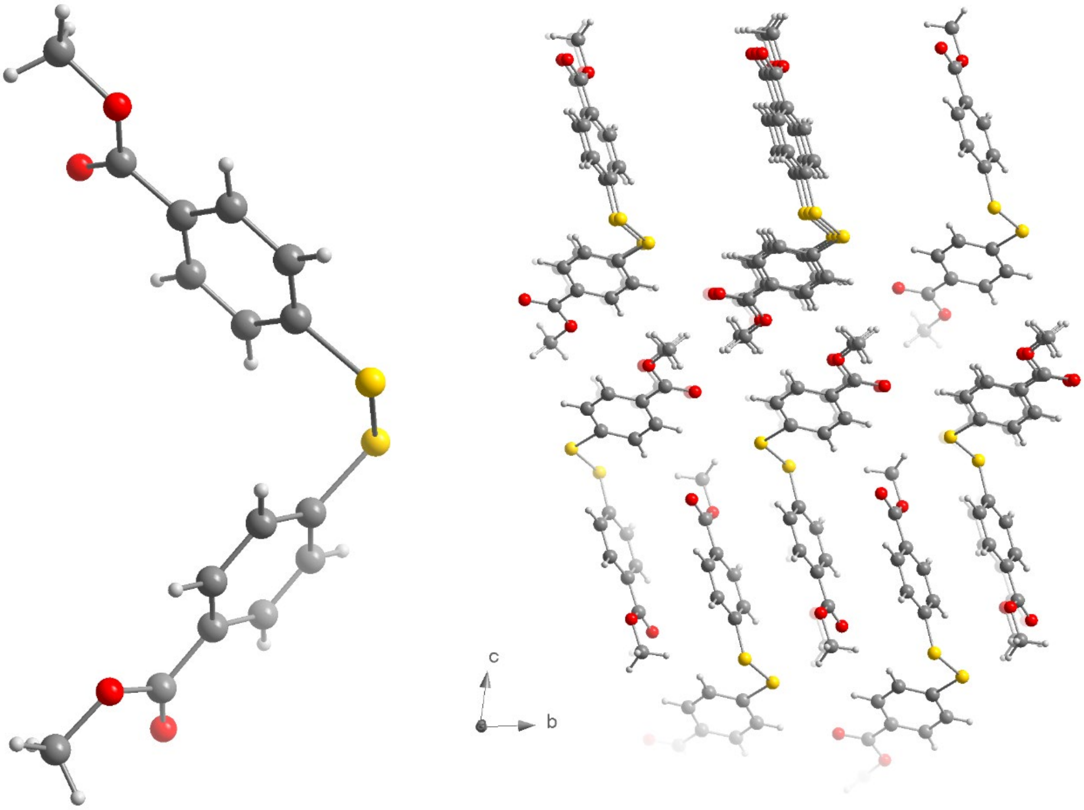

Figure S1. Representations of the crystallographic structure of compound **2**. On the left the molecule ($(p\text{-SPhCO}_2\text{Me})_2$) and on the right its packing. Yellow, red, gray and white spheres are sulfur, oxygen, carbon and hydrogen atoms, respectively.

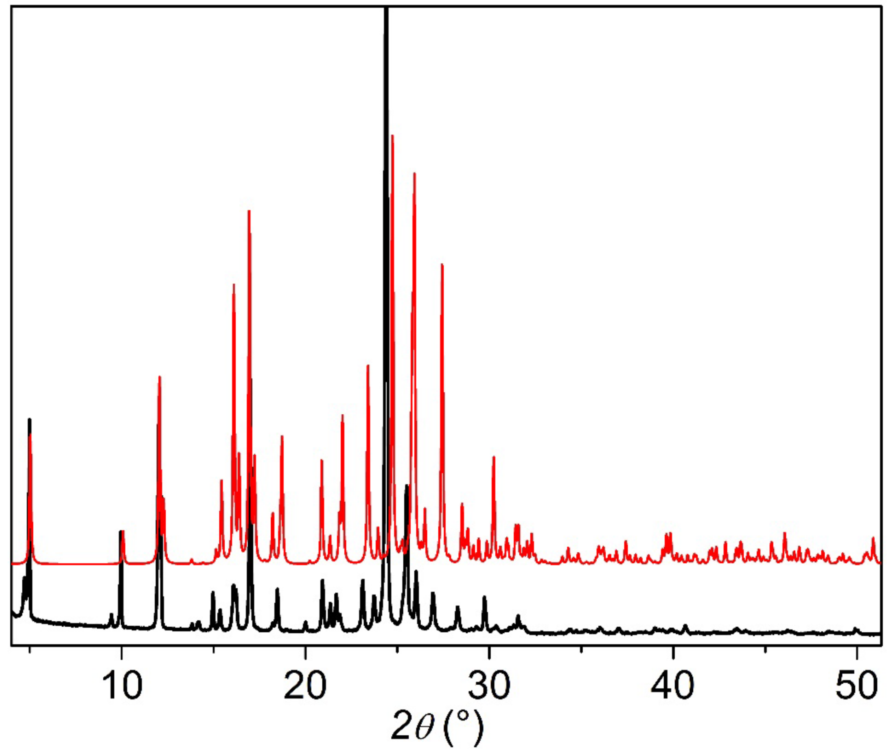

Figure S2. Observed (black) and calculated (red) XRD patterns of compound **2** $(p\text{-SPhCO}_2\text{Me})_2$.

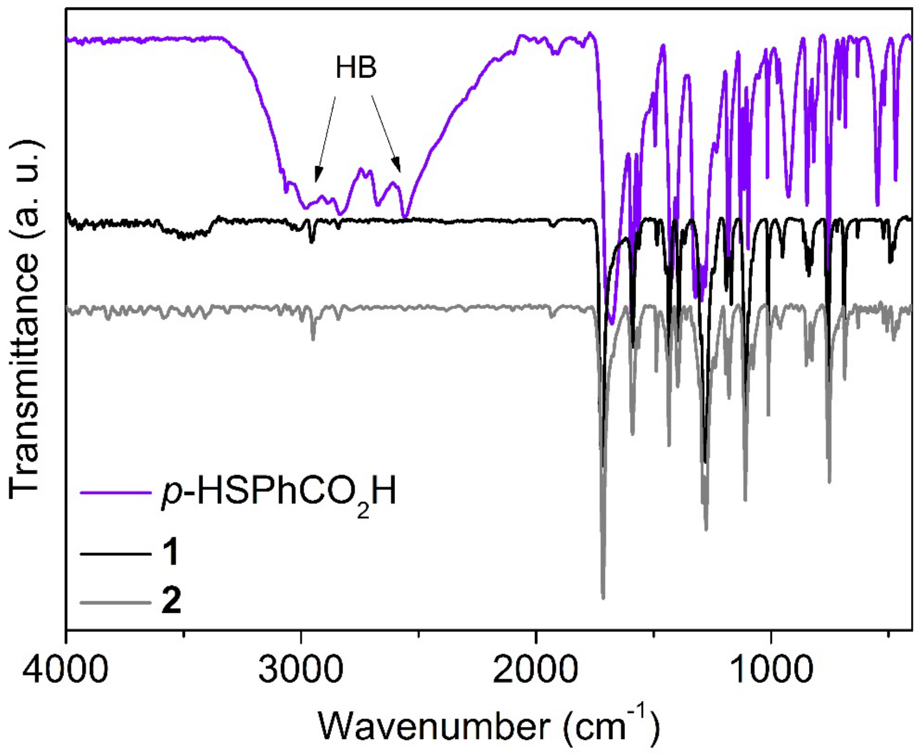

Figure S3. FT-IR spectra of *p*-HSPhCO$_2$H and **1** and **2** compounds. Presence of ν(OH) bands at 2560, 2670, 2830, 2980 and 3065 cm^{-1} on *p*-HSPhCO$_2$H are due to hydrogen bonds (HB) between the carboxylic acid functions. They are absent for **1** and **2** pointing out the complete esterification.

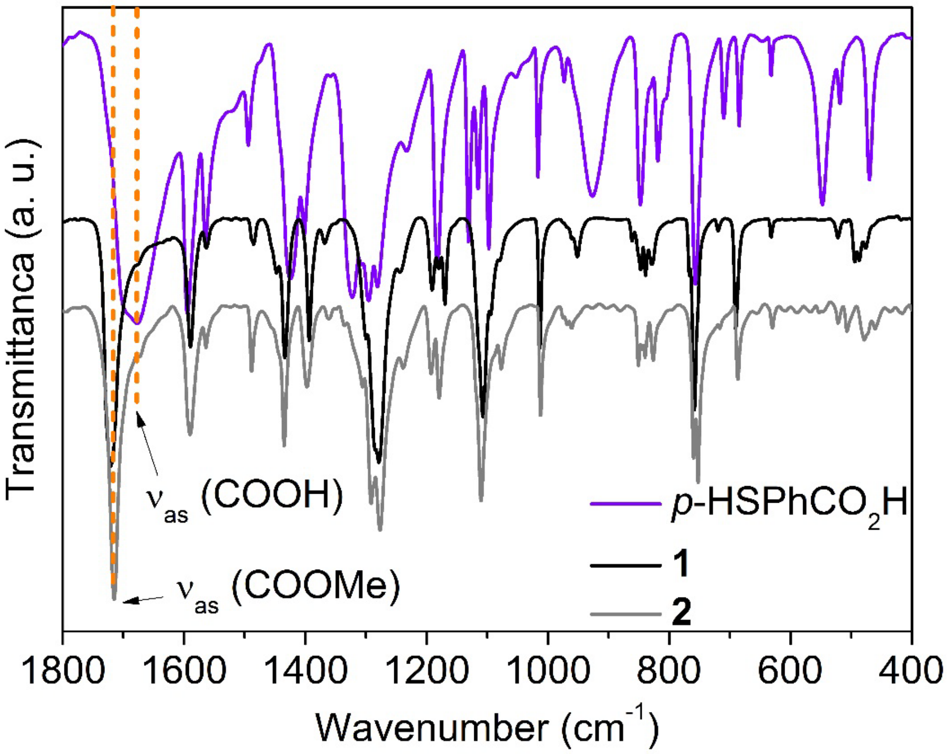

Figure S4. Zoom on the FT-IR spectra of *p*-HSPhCO$_2$H and **1** and **2** compounds. Antisymmetric vibrations of CO are present at 1677 cm^{-1} for *p*-HSPhCO$_2$H and at 1721 and 1715 cm^{-1} for ester-based **1** and **2** compounds, respectively.

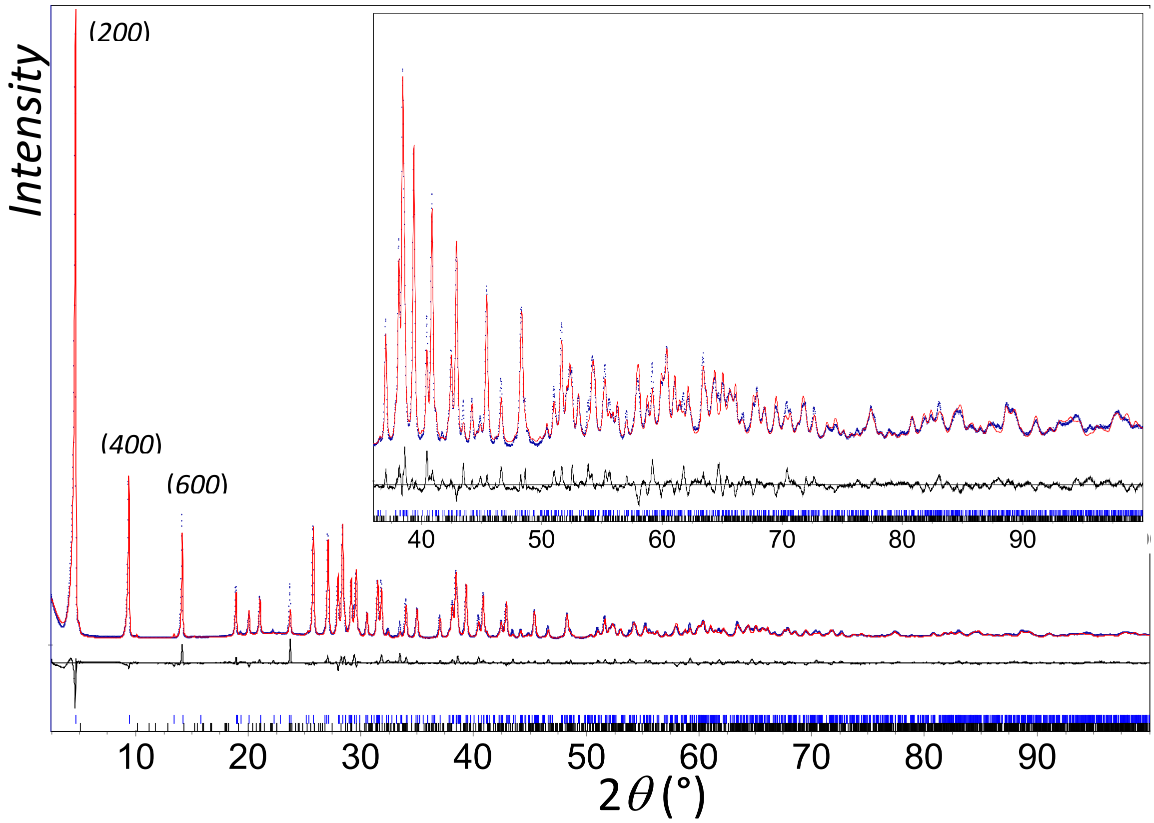

Figure S5. Final Rietveld plot of $[Au(p\text{-}SPhCO_2Me)]_n$ showing observed (blue circles), calculated (red line), and difference (black line) curves. A zoom at high angles is shown as inset. Black ticks correspond to the compound **2** impurity. First (*h00*) reflections are assigned.

Table S2. Selected distances (Å) and angles (°) from the crystallographic structure of compound **1**.

Au-Au (inter)	3.199(5)
Au-Au (intra)†	3.509(5)
Au-S	2.307(1) 2.375(1)
Au-S-Au	97.09(2)
S-Au-S	177.47(4)
Au-Au-Au (inter)	168.34(1)
Au-Au-Au (intra)†	176.51(3)

† bridged by sulfur atoms

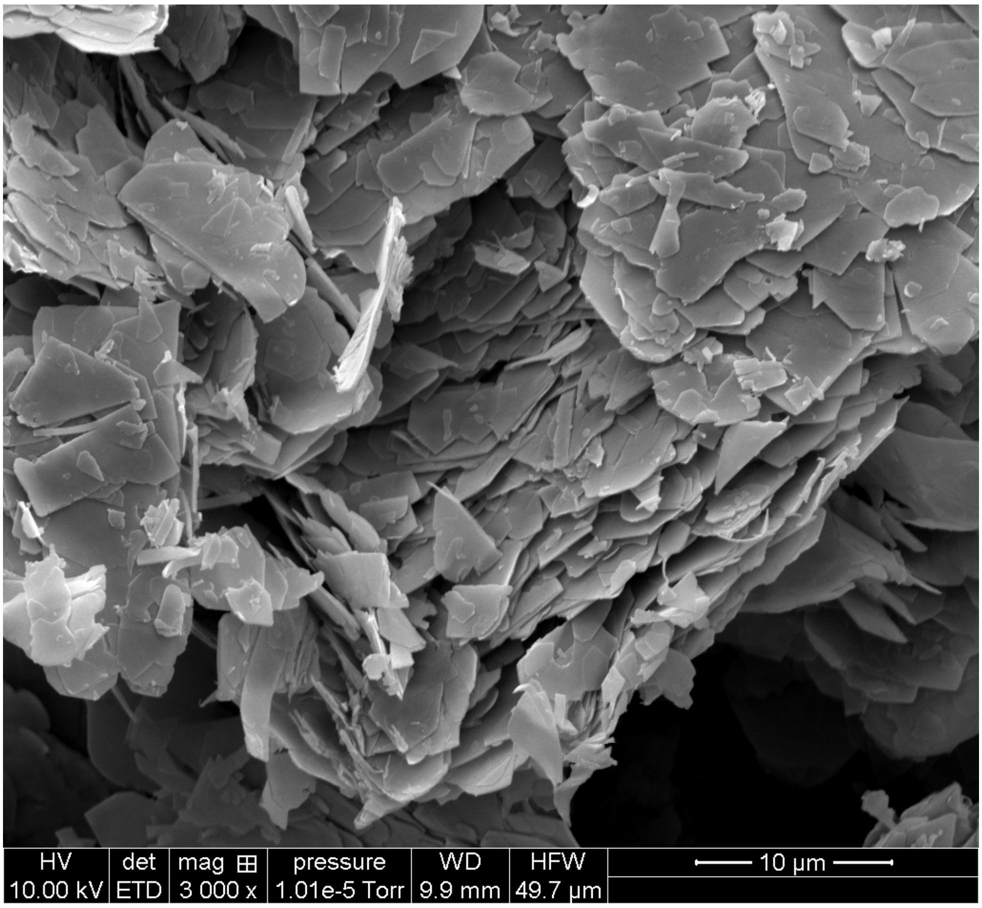

Figure S6. SEM image of compound **1**.

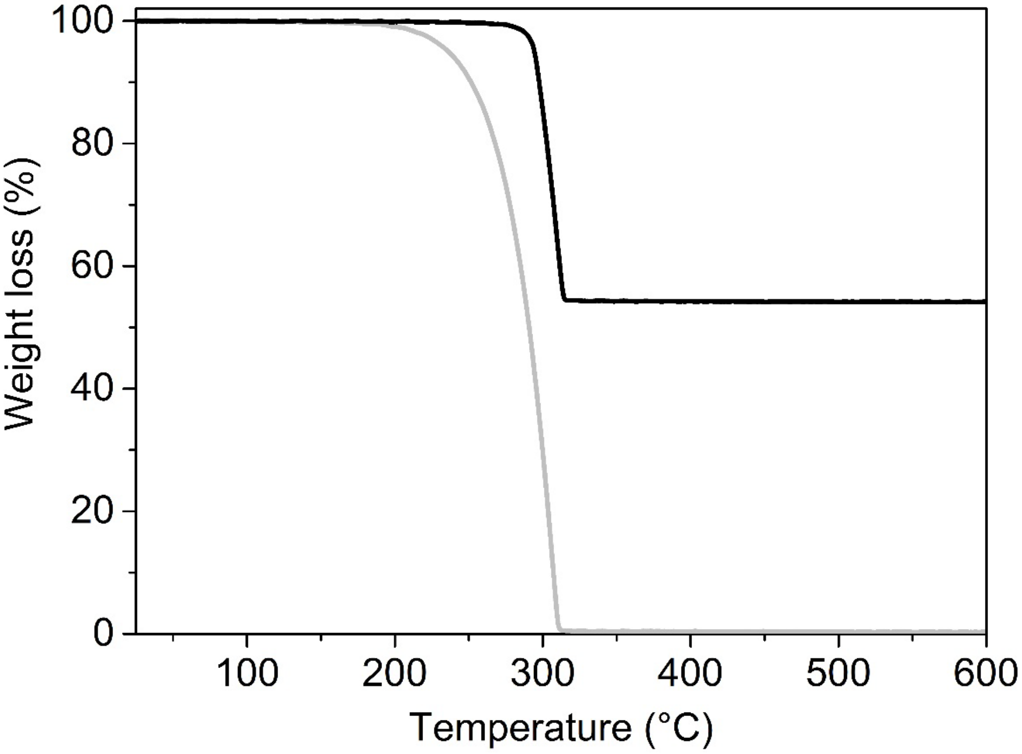

Figure S7. TGA of compounds **1** (black) and **2** (grey) carried out under air at 10 °C/min.

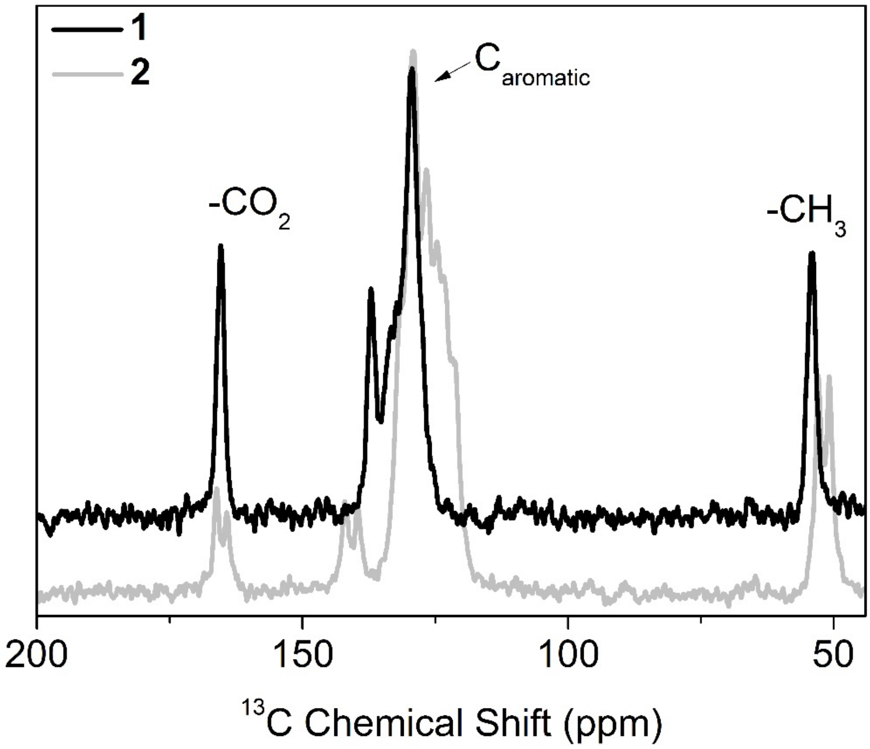

Figure S8. ^{13}C solid-state NMR of compounds **1** and **2**.

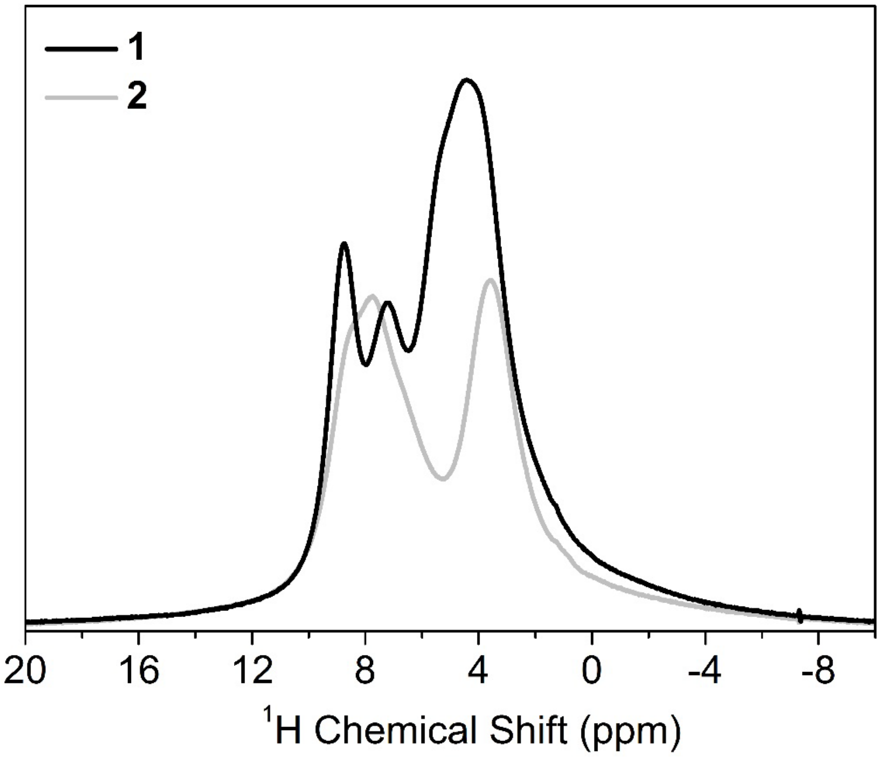

Figure S9. ^{1}H solid-state NMR of compounds **1** and **2**.

Table S3. XPS data (quantification and position) of gold, sulfur, oxygen and carbon binding energies of compound **1**.

	Au 4f		**S 2p**		**O 1s**	**C 1s**
Quantification (mol%)	9.25		8.11		14.97	67.67
Molar ratio [theoretical]	1 [1]		0.9 [1]		1.6 [2]	7.3 [8]
Peak position (eV)	**Au 4f$_{7/2}$**	**Au 4f$_{5/2}$**	**S 2p$_{3/2}$**	**S 2p$_{1/2}$**	**O 1s**	**C 1s**
	84.9	88.6	163.3	164.5	531.7 [C=O] 533.4 [C-OMe]	284.7 [C_6H_4] 286.1 [CH_3] 288.6 [CO_2]

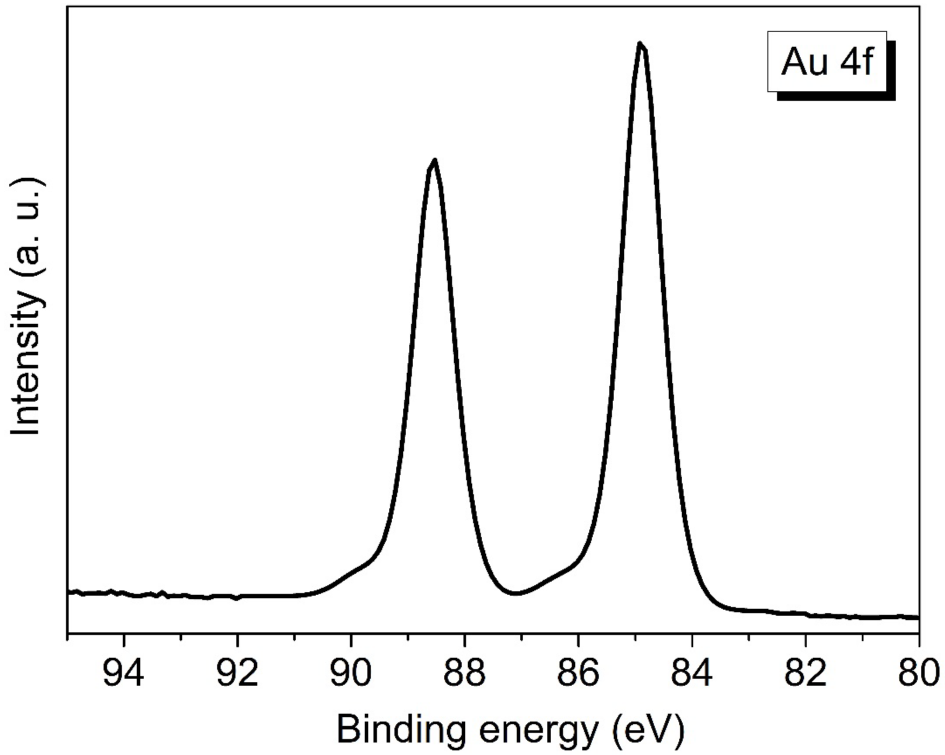

Figure S10. High resolution XPS spectrum of Au 4f binding energies of compound **1**.

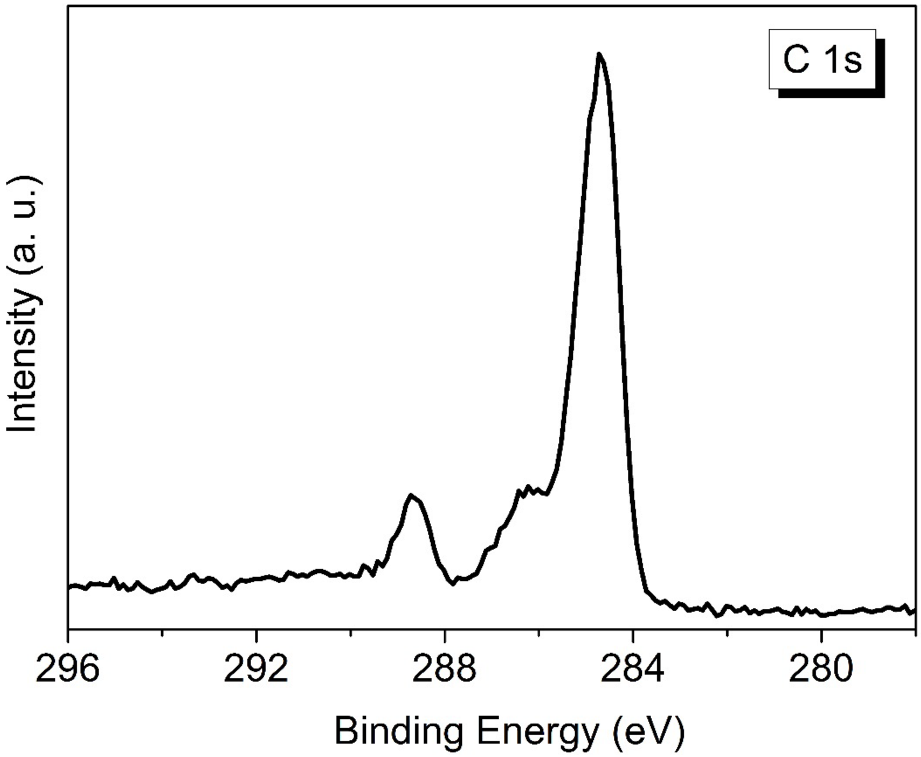

Figure S11. High resolution XPS spectrum of C 1s binding energies of compound **1**.

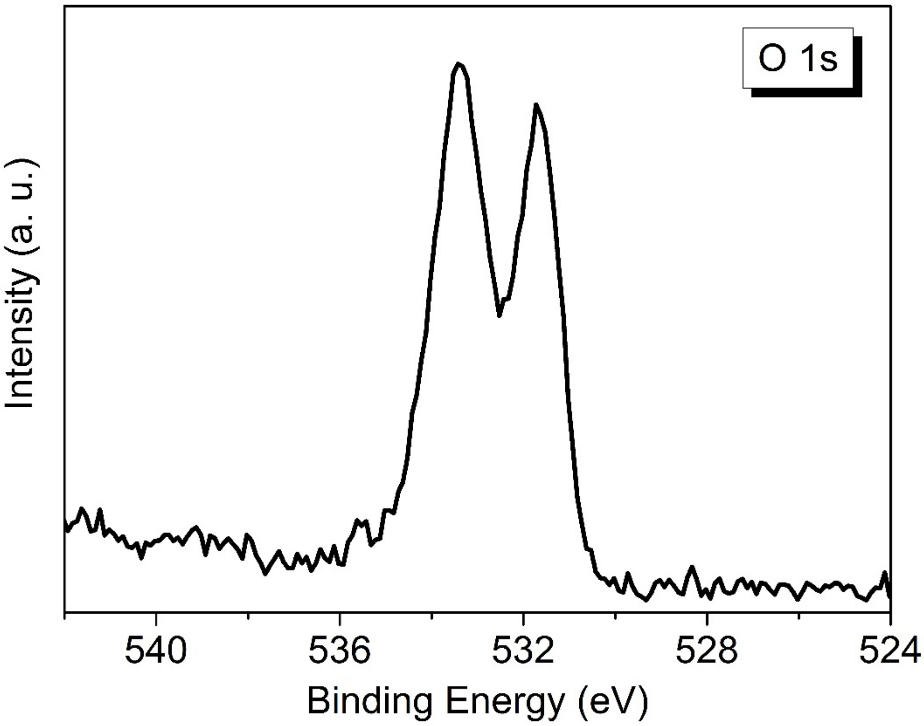

Figure S12. High resolution XPS spectrum of O 1s binding energies of compound **1**.

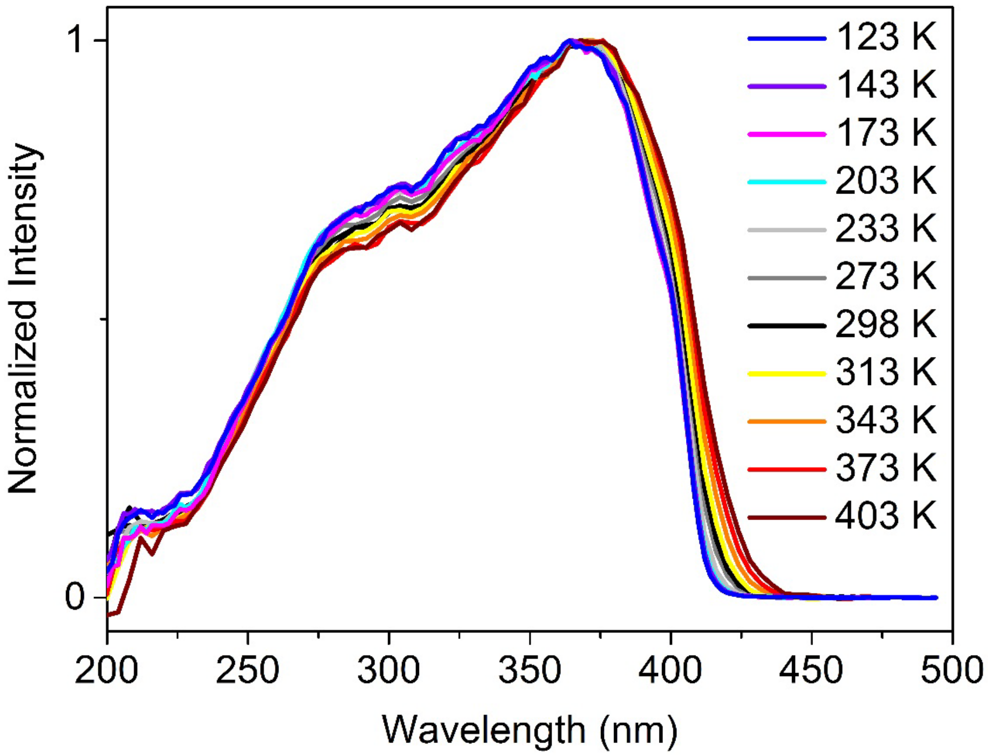

Figure S13. Normalized intensities of excitation spectra (λ_{em} = 650 nm) of compound **1** carried out in solid-state with the temperature.

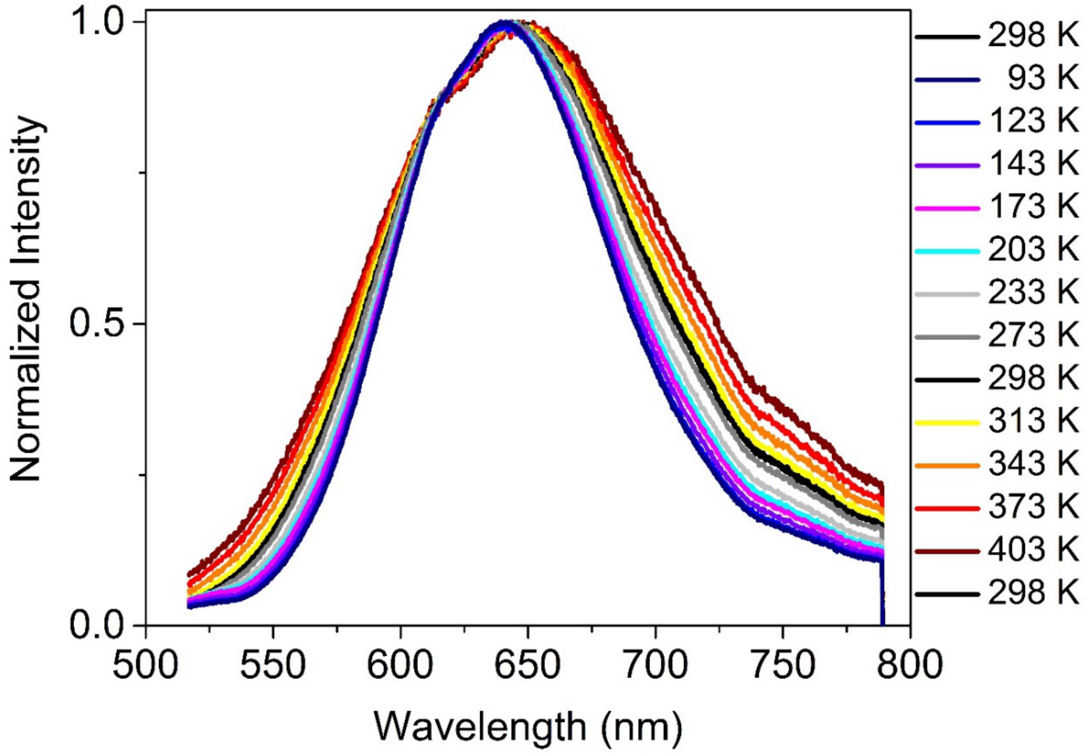

Figure S14. Normalized intensity of emission spectra (λ_{ex} = 320 nm) of compound **1** carried out in solid-state with the temperature.

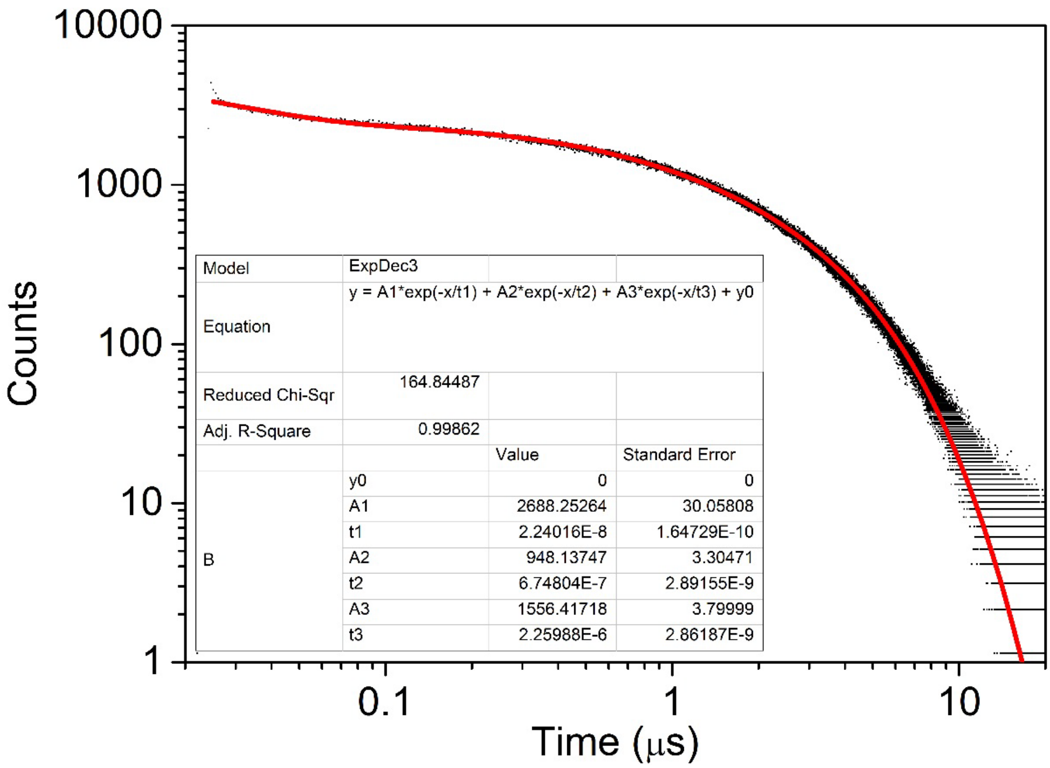

Model	ExpDec3		
Equation	y = A1*exp(-x/t1) + A2*exp(-x/t2) + A3*exp(-x/t3) + y0		
Reduced Chi-Sqr	164.84487		
Adj. R-Square	0.99862		
		Value	Standard Error
B	y0	0	0
	A1	2688.25264	30.05808
	t1	2.24016E-8	1.64729E-10
	A2	948.13747	3.30471
	t2	6.74804E-7	2.89155E-9
	A3	1556.41718	3.79999
	t3	2.25988E-6	2.86187E-9

Figure S15. Luminescence lifetime decay (λ_{ex} = 379 nm) of compound **1** (black) carried out in solid-state at 298 K with a triexponential fit (red).

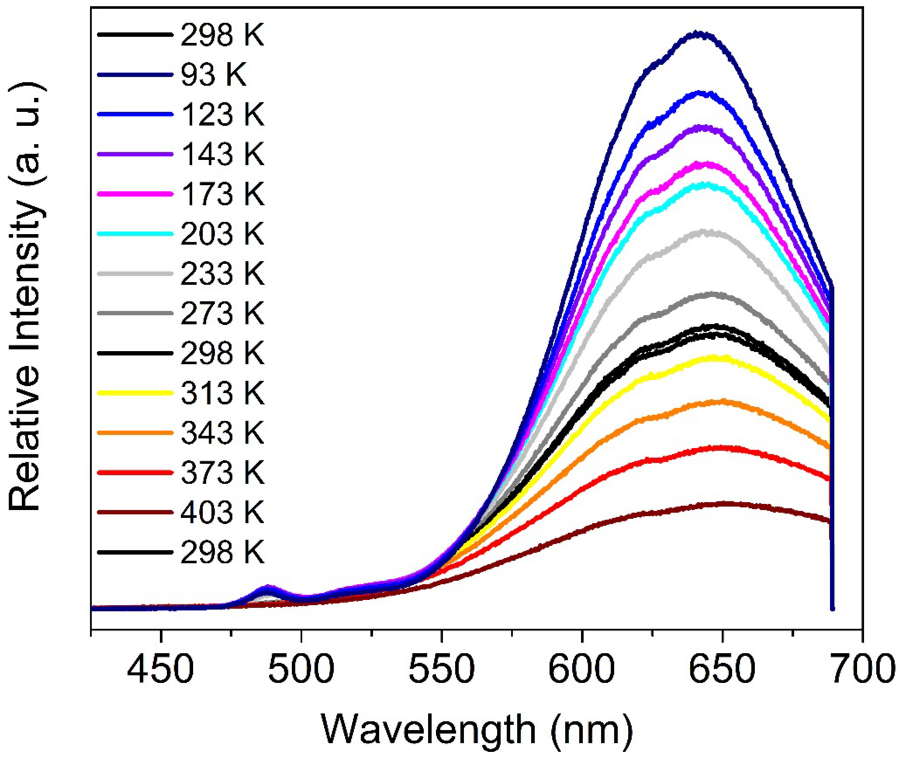

Figure S16. Solid-state emission spectra (λ_{ex} = 320 nm) of compound **1** with the temperature.

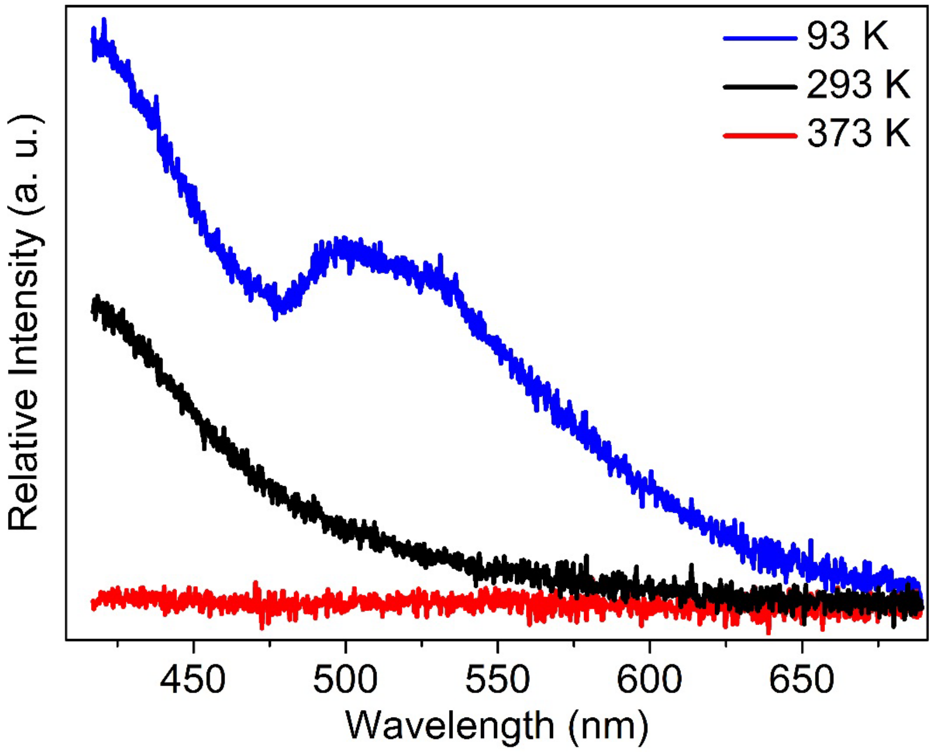

Figure S17. Emission spectra (λ_{ex} = 320 nm) of the free ligand *p*-HSPhCO$_2$Me, at different temperatures.

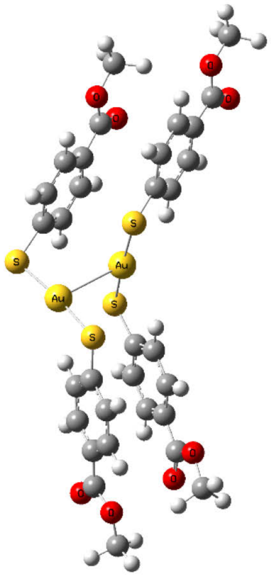

Figure S18. $[\{Au(SPhCO_2Me)_2\}_2]^{2-}$ optimised at RI-MP2 level of theory.

Table S4. Selected distances (Å) and angles (°) from the optimized structure of model system $[\{Au(SPhCO_2Me)_2\}_2]^{2-}$.

Au-Au	2.96
Au-S	2.285 2.288
S-Au-S	171.2 174.2
S-C	1.746 1.741
Au-S-C	104.5 106.0
C-O	1.354 1.372
C=O	1.216 1.221

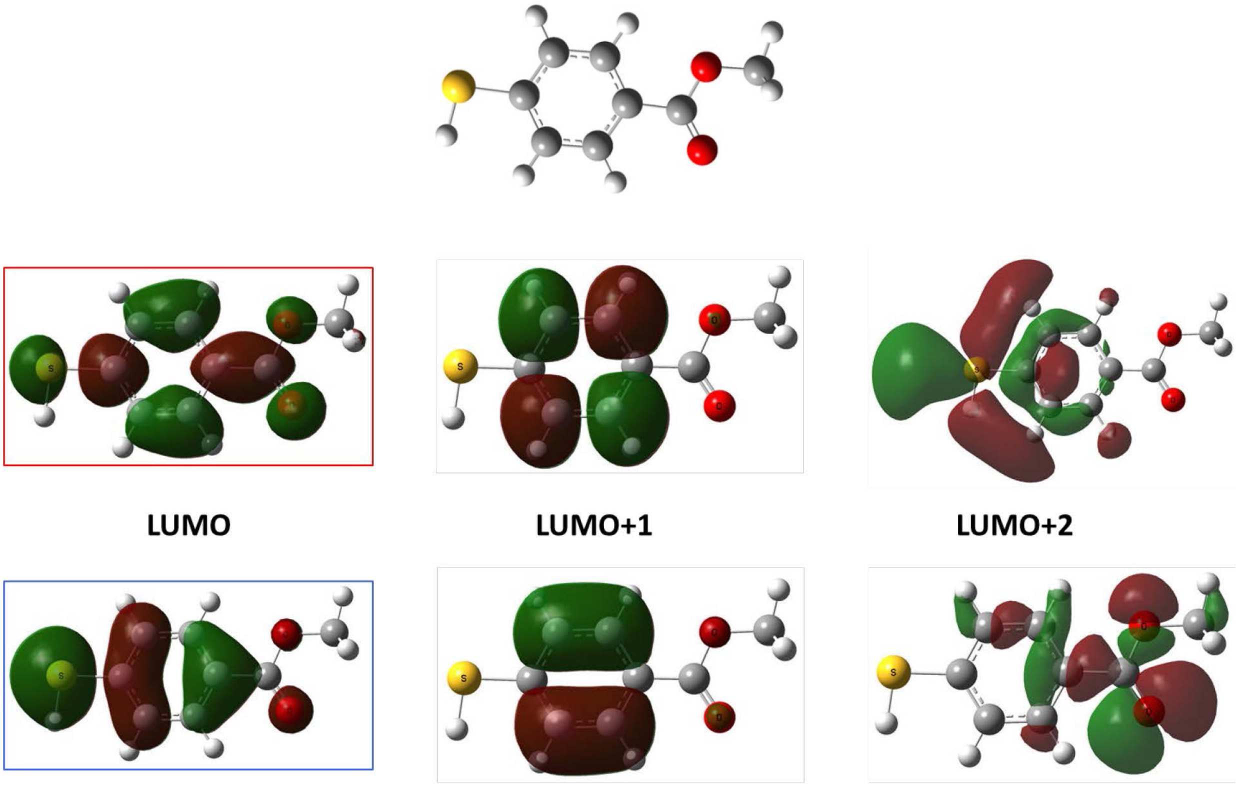

LUMO LUMO+1 LUMO+2

HOMO HOMO-1 HOMO-2

Figure S19. DFT/pbe1pbe optimization and frontier orbitals of the model *p*-$HSPhCO_2Me$.

Table S5. Contributions of the substituent in the molecular orbitals of the model *p*-$HSPhCO_2Me$ at DFT/pbe1pbe level of theory.

MO	*SH*	*Ph*	*CO_2Me*
L+2	72	27	1
L+1	0	98	1
LUMO	**6**	**64**	**31**
HOMO	**48**	**48**	**4**
H-1	0	99	1
H-2	0	10	90

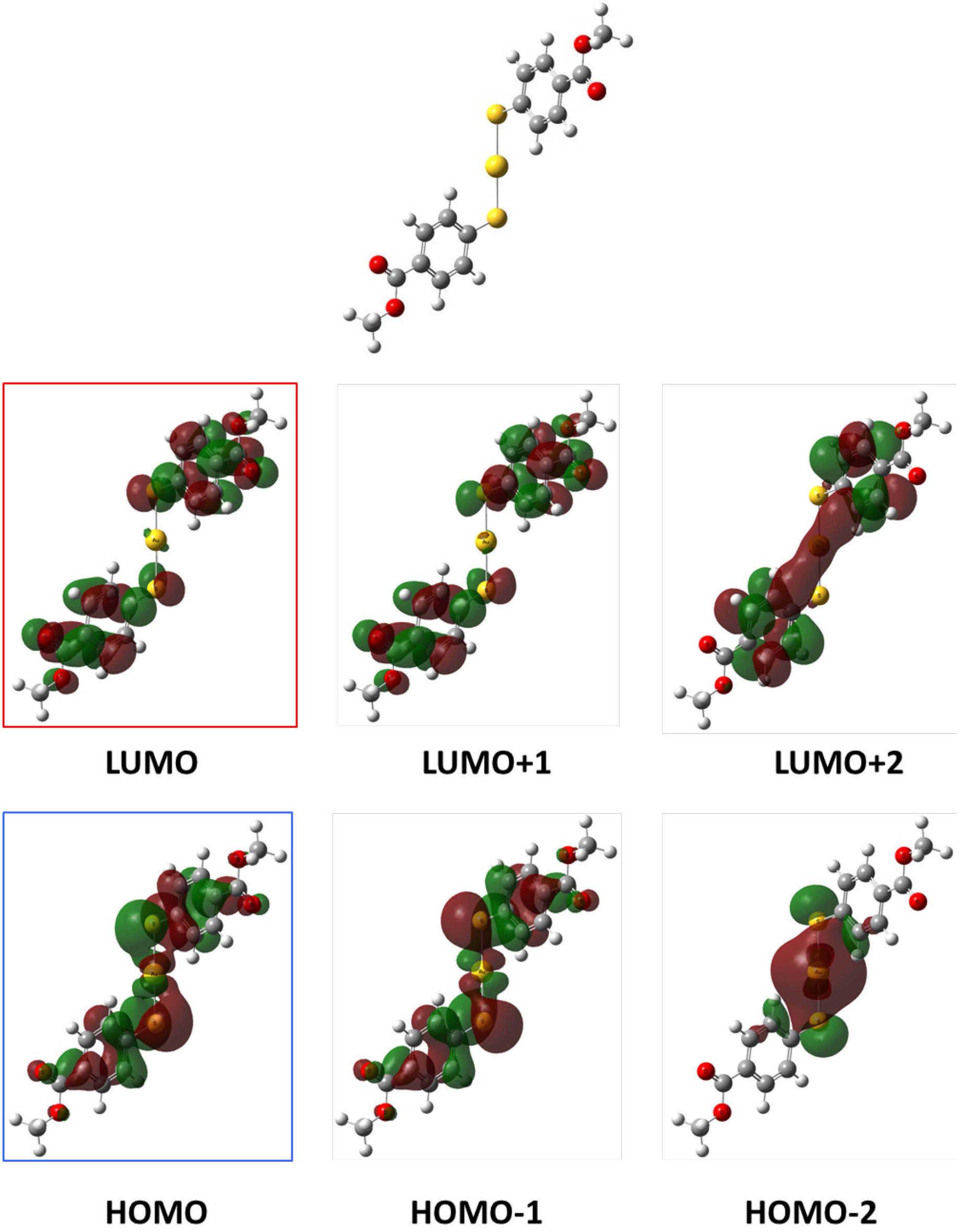

Figure S20. DFT/pbe1pbe optimization and frontier orbitals of the model [Au(SPhCO$_2$Me)$_2$]$^-$.

Table S6. Contributions of the substituent in the molecular orbitals of the model $[Au(SPhCO_2Me)_2]^-$ at DFT/pbe1pbe level of theory.

MO	*Au*	*S*	*Ph*	*CO_2Me*
L+3	15	0	86	0
L+2	16	0	85	0
L+1	2	7	54	36
LUMO	**3**	**7**	**54**	**36**
HOMO	**10**	**56**	**30**	**4**
H-1	10	56	30	4
H-2	71	26	4	0
H-3	10	83	7	0

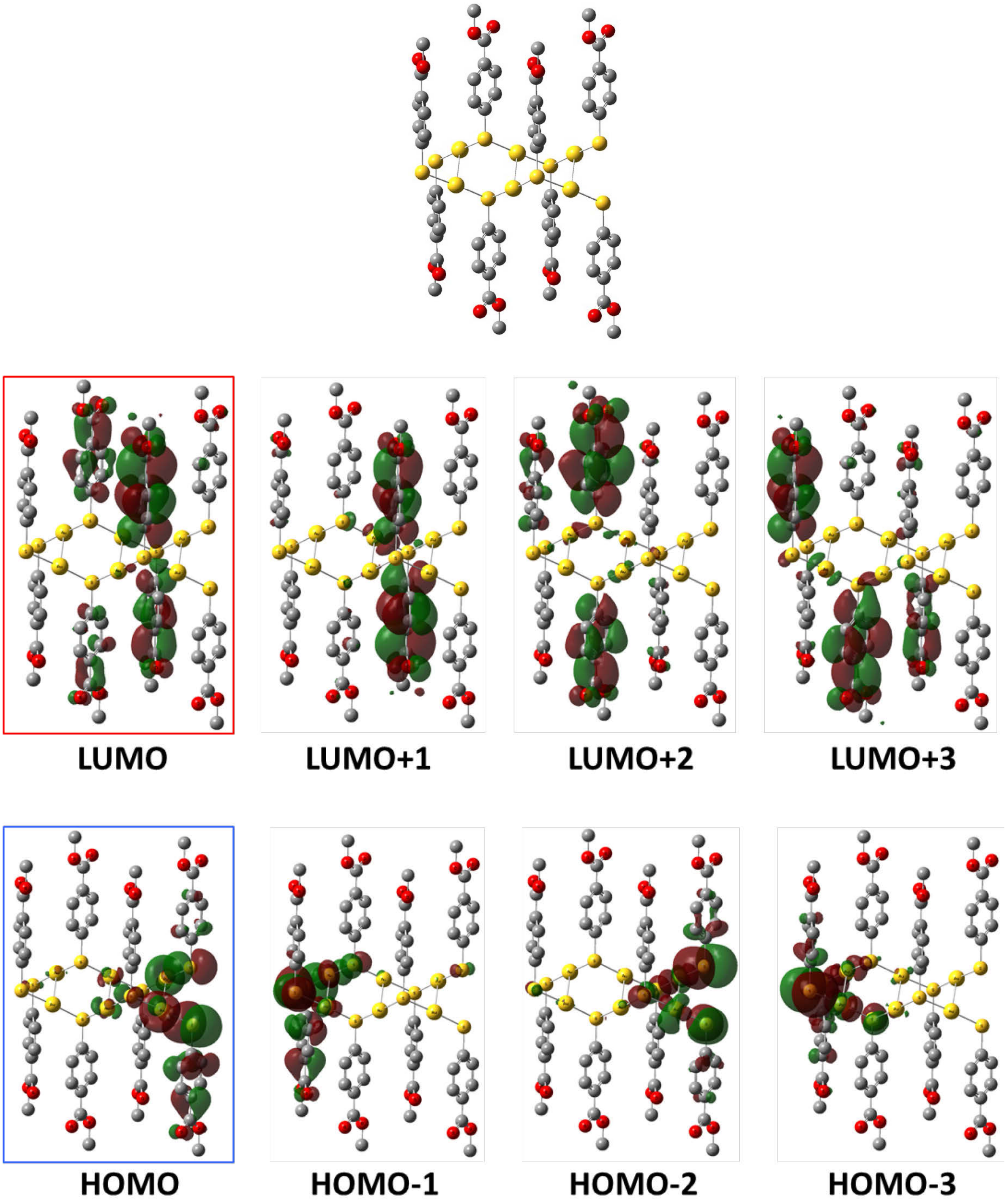

Figure S21. DFT/pbe1pbe single-point calculation and frontier orbitals of the model $[Au_6(SPhCO_2Me)_8]^{2-}$ bearing aurophilic interactions between the two $[Au_3(SPhCO_2Me)_4]^-$ chains along the *b* axis.

Table S7. Contributions of the substituent in the molecular orbitals of the model $[Au_6(SPhCO_2Me)_8]^{2-}$ at DFT/pbe1pbe level of theory.

MO	*Au*	*S*	*Ph*	*CO_2Me*
L+3	6	2	55	37
L+2	4	4	56	35
L+1	6	3	56	36
LUMO	**4**	**3**	**56**	**36**
HOMO	**23**	**60**	**15**	**2**
H-1	14	70	14	2
H-2	19	73	8	1
H-3	16	75	8	1

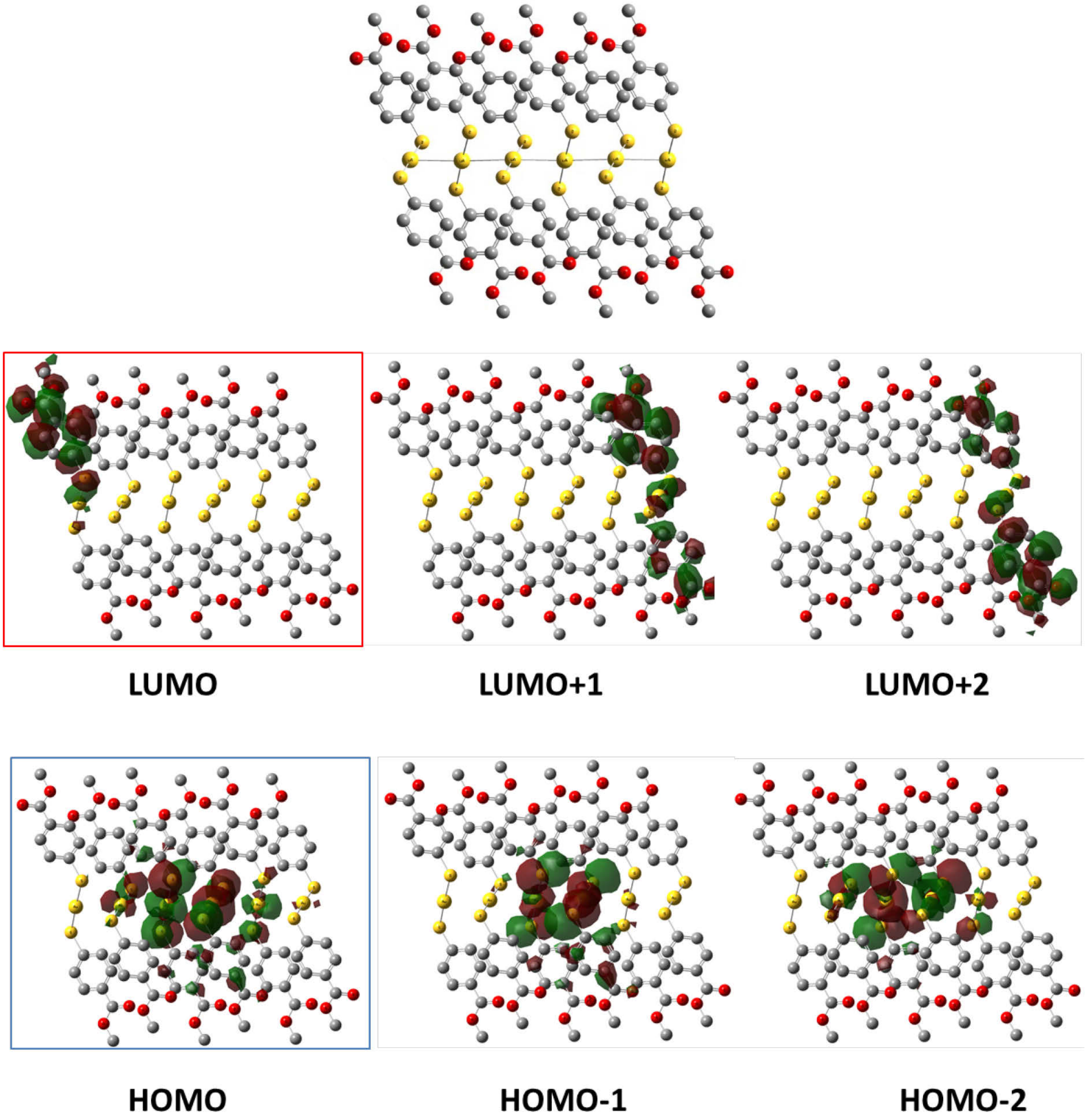

Figure S22. DFT/pbe1pbe single-point calculation and frontier orbitals of the model $[Au_6(SPhCO_2Me)_{12}]^{6-}$ bearing 1D aurophilic interactions along the *c* axis.

Table S8. Contributions of the substituent in the molecular orbitals of the model $[Au_6(SPhCO_2Me)_{12}]^{6-}$ at DFT/pbe1pbe level of theory.

MO	***Au***	***S***	***Ph***	***CO_2Me***
L+2	3	4	43	49
L+1	6	3	46	45
LUMO	**6**	**2**	**43**	**50**
HOMO	**36**	**49**	**12**	**3**
H-1	18	71	9	1
H-2	34	59	6	1

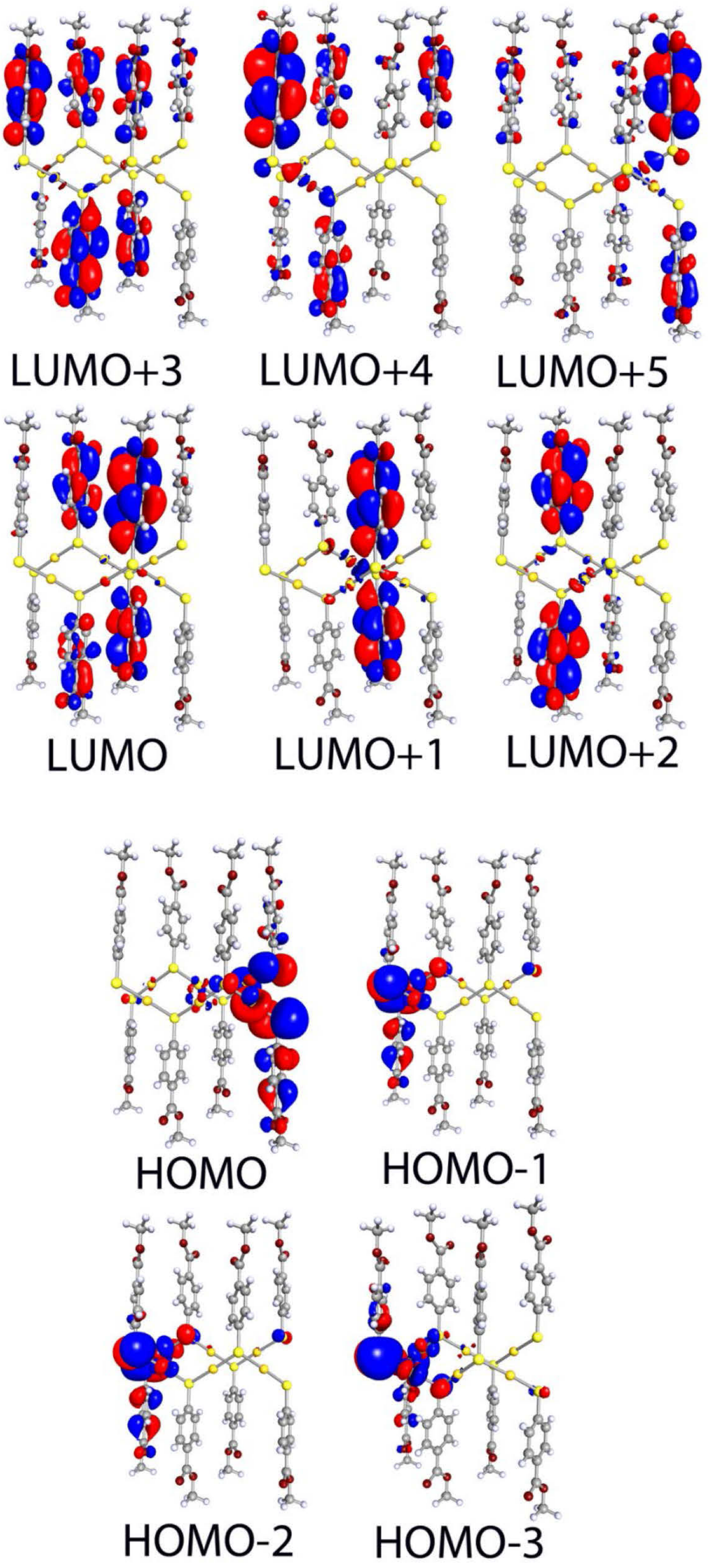

LUMO+3 LUMO+4 LUMO+5

LUMO LUMO+1 LUMO+2

HOMO HOMO-1

HOMO-2 HOMO-3

Figure S23. RI-DFT/pbe single-point calculation and frontier orbitals of the model $[Au_6(SPhCO_2Me)_8]^{2-}$.

Table S9. Contributions of the substituent in the molecular orbitals of the model $[Au_6(SPhCO_2Me)_8]^{2-}$ at RI-DFT/pbe level of theory.

MO	*Au*	*S*	*Ph*	*CO_2Me*
L+5	5	2	53	40
L+4	4	2	55	39
L+3	5	1	57	37
L+2	4	1	60	35
L+1	5	2	58	35
LUMO	**6**	**0**	**59**	**35**
HOMO	**21**	**64**	**14**	**1**
H-1	13	75	11	1
H-2	17	78	5	0
H-3	17	76	7	0

Table S10. RI-DFT/TDDFT calculations of the lowest singlet-triplet excitation and first 10 singlet-singlet excitations.

Excitation	λ_{em} (nm) / osc strength[a]	Transition (main contributions)[b]
$S_0 \rightarrow T_1$	458 / 0.63	HOMO → LUMO+5 (28.0) HOMO → LUMO+6 (23.2) HOMO → LUMO+7 (12.1)
$S_0 \rightarrow S_1$	425.5 / 0.0007	HOMO → LUMO (46.3) HOMO-2 → LUMO+1 (21.4) HOMO-2 → LUMO (20.7)
$S_0 \rightarrow S_2$	424.7 / 0.0015	HOMO → LUMO+1 (71.4) HOMO → LUMO (11.8)
$S_0 \rightarrow S_3$	417.3 / 0.0077	HOMO-3 → LUMO+4 (46.3) HOMO-3 → LUMO+3 (21.4) HOMO-1 → LUMO+3 (20.7) HOMO-1 → LUMO+4 (20.7)
$S_0 \rightarrow S_4$	412.2 / 0.025	HOMO-2 → LUMO (27.0) HOMO-2 → LUMO+5 (23.1) HOMO → LUMO+5 (12.1)
$S_0 \rightarrow S_5$	409.8 / 0.0066	HOMO-2 → LUMO+2 (38.2) HOMO → LUMO (24.0) HOMO → LUMO+5 (10.9) HOMO-2 → LUMO+2 (10.3)
$S_0 \rightarrow S_6$	402.3 / 0.011	HOMO-1 → LUMO (59.4) HOMO-1 → LUMO+2 (15.0)
$S_0 \rightarrow S_7$	400.4 / 0.031	HOMO-2 → LUMO+1 (32.4) HOMO-2 → LUMO (22.9) HOMO-2 → LUMO+5 (19.8)
$S_0 \rightarrow S_8$	400.0 / 0.0049	HOMO-1 → LUMO+2 (78.4) HOMO-1 → LUMO (12.4)
$S_0 \rightarrow S_9$	391.9 / 0.0054	HOMO-1 → LUMO+1 (71.1) HOMO-3 → LUMO (17.9)
$S_0 \rightarrow S_{10}$	390.6 / 0.0012	HOMO → LUMO+2 (75.4) HOMO → LUMO+3 (10.2)

[a] Oscillator strength (f) shows the mixed representation of both velocity and length representations. [b] Value is 2 x |coeff|^2 x 100.

References

[1]. *CrysAlisPro, Agilent Technologies, Version 1.171.34.49 (release 20-01-2011 CrysAlis171.NET).*

[2]. R. C. Clark; J. S. Reid, *Acta Cryst., Sect. A*, **1995**, *51*, 887.

[3]. A. Altmore; M. C. Burla; M. Camalli; G. L. Cascarano; C. Giacovazzo; A. Guagliardi; A. Grazia; G. Moliterni; G. Polidori; R. Spagna, *J. Appl. Cryst.*, **1999**, *32*, 115.

[4]. P. W. Betteridge; J. R. Carruthers; R. I. Cooper; K. Prout; D. J. Watkin, *J. Appl. Cryst.*, **2003**, *36*, 1487.

[5]. *Topas V4.2: General Profile and Structure Analysis Software for Powder Diffraction Data, Bruker AXS Ltd, 2008.*

[6]. S. Mishra; E. Jeanneau; G. Ledoux; S. Daniele, *Inorg. Chem.*, **2014**, *53*, 11721.

[7]. Gaussian 09, Revision A.1, M. J. Frisch, G. W. Trucks, H. B. Schlegel, G. E. Scuseria, M. A. Robb, J. R. Cheeseman, G. Scalmani, V. Barone, B. Mennucci, G. A. Petersson, H. Nakatsuji, M. Caricato, X. Li, H. P. Hratchian, A. F. Izmaylov, J. Bloino, G. Zheng, J. L. Sonnenberg, M. Hada, M. Ehara, K. Toyota, R. Fukuda, J. Hasegawa, M. Ishida, T. Nakajima, Y. Honda, O. Kitao, H. Nakai, T. Vreven, J. A. Montgomery, Jr., J. E. Peralta, F. Ogliaro, M. Bearpark, J. J. Heyd, E. Brothers, K. N. Kudin, V. N. Staroverov, R. Kobayashi, J. Normand, K. Raghavachari, A. Rendell, J. C. Burant, S. S. Iyengar, J. Tomasi, M. Cossi, N. Rega, J. M. Millam, M. Klene, J. E. Knox, J. B. Cross, V. Bakken, C. Adamo, J. Jaramillo, R. Gomperts, R. E. Stratmann, O. Yazyev, A. J. Austin, R. Cammi, C. Pomelli, J. W. Ochterski, R. L. Martin, K. Morokuma, V. G. Zakrzewski, G. A. Voth, P. Salvador, J. J. Dannenberg, S. Dapprich, A. D. Daniels, Ö. Farkas, J. B. Foresman, J. V. Ortiz, J. Cioslowski, and D. J. Fox, Gaussian, Inc., Wallingford CT, **2009**.

[8]. D. Andrae; U. Häussermann; M. Dolg; H. Stoll; H. Preuss, *Theor. Chem. Acc.*, **1990**, *77*, 123.

[9]. A. Bergner; M. Dolg; W. Küchle; H. Stoll; H. Preuss, *Mol. Phys.*, **1993**, *80*, 1431.

[10]. S. Huzinaga, *Gaussian Basis Sets for Molecular Calculations; Elsevier: Amsterdam*, **1984**, 16.

[11]. S. Huzinaga, *J. Chem. Phys.*, **1965**, *42*, 1293.

[12]. C. Adamo; V. Barone, *J. Chem. Phys.*, **1999**, *110*, 6158.

[13]. N. M. O'Boyle; A. L. Tenderholt; K. M. Langner, *J. Comp. Chem.*, **2008**, *29*, 839.

[14]. R. Ahlrichs; M. Bär; M. Häser; H. Horn; C. Kölmel, *Chem. Phys. Lett.*, **1989**, *162*, 165.

[15]. J. P. Perdew; K. Burke; M. Ernzerhof, *Phys. Rev. Lett.*, **1996**, *77*, 3865.

[16]. S. Grimme; J. Antony; S. Ehrlich; H. Krieg, *J. Chem. Phys.*, **2010**, *132*, 154104.

[17]. M. Feyereisen; G. Fitzgerald; A. Komornicki, *Chem. Phys. Lett.*, **1993**, *208*, 359.

[18]. A. Schäfer; C. Huber; R. Ahlrichs, *J. Chem. Phys.*, **1994**, *100*, 5829.

[19]. F. Weigend; R. Ahlrichs, *Phys. Chem. Chem. Phys.*, **2005**, *7*, 3297.